Abnormal threshold properties of fluxon propagation in a resistively coupled Josephson transmission line

doi: 10.1103/PhysRevB.35.4764

Abnormal threshold properties of fluxon propagation in a resistively coupled Josephson transmission line

Junsaku Nitta and Azusa Matsuda
Nippon Telegraph and Telephone Corporation, Electrical Communications Laboratories, Musashino-shi, Tokyo 180, Japan
(Received 22 September 1986)

Fluxon-propagation threshold properties in a resistively coupled Josephson transmission line are experimentally investigated by use of a direct measurement system for a single fluxon observation. A nontransmission bias-current region is observed between the high- and low-bias-current transmission regions. These unexpected threshold properties can be interpreted in terms of an interaction among damping oscillations. Experimentally obtained properties approximately agree with numerical simulations.

I. INTRODUCTION

Recently, the soliton concept in nonlinear dispersive waves has been applied in solid-state physics.[1,2] In particular, a sine-Gordon soliton is widely used as a model for dislocations in crystals,[3] domain walls in ferromagnets,[4] excitations in the charge-density-wave (CDW) state[5] and a quantized magnetic flux (fluxon) in a Josephson transmission line (JTL). However, in most cases, the identification of a soliton mode sometimes becomes controversial. This is because a soliton in the solid-state physics is a microscopic object, and perturbational effects may significantly change its characteristics.

The most direct method for identifying a soliton is to observe a soliton wave form profile. A JTL is a suitable system for experimental investigation of sine-Gordon soliton properties, because a fluxon carries a quantized magnetic flux of an amount sufficient to observe ($\Phi_0 = 2\times 10^{-15}$ V s).

The measurement systems for observing a single fluxon have been developed by using a minicomputer signal processing technique[6] and a Josephson sampling technique.[7] The fundamental soliton properties in a JTL have been directly clarified by these systems,[8,9] and their dependence on input pulse height and the perturbational effects have been investigated experimentally. The results have agreed with numerical and perturbation analyses.[10,11]

In this paper, a resistively coupled JTL (RCJ) has been investigated for the purpose of clarifying the boundary condition effect and the ability to control fluxons. An RCJ consists of two JTL's interconnected by a coupling resistor. It has been previously reported[12,13] that the incident fluxon transmits, reflects, or annihilates at the resistor. These properties depend on the bias currents fed into the respective JTL's. The incident fluxon is more easily transmitted through the coupling resistor at the higher bias-current levels, because they provide a fluxon with Lorentz force. However, through the present experiment, unexpected threshold properties have been observed in the multifluxon input cases. These properties are discussed in the following sections.

II. NUMERICAL ANALYSIS

An RCJ consists of two JTL's (JTL1 and JTL2) interconnected by a coupling resistor R_c. The equivalent circuit of the RCJ is shown in Fig. 1. At the coupling resistor, the flux quantization condition does not hold. The behaviors of propagating fluxons are thought to be strongly affected by the resistor. In this section, fluxon threshold properties on the RCJ are investigated by numerical analysis.

A. JTL parameters and boundary condition

It is well known that a JTL obeys the sine-Gordon equation. This equation has a kink solution which corresponds to a quantized magnetic flux (fluxon) in a JTL. However, an actually fabricated JTL, taking perturbational losses into account, obeys the following modified sine-Gordon equation:

$$\frac{\partial^2\varphi}{\partial x^2}-\frac{\partial^2\varphi}{\partial t^2}=\sin\varphi+\alpha\frac{\partial\varphi}{\partial t}-\beta\frac{\partial^3\varphi}{\partial x^2\partial t}-\gamma\ , \tag{1}$$

where α, β, and γ are associated with quasiparticle tunneling loss, superconducting rf loss, and an artificially provided bias current, respectively. In the equation, space and time are normalized by Josephson penetration depth λ_j ($=[\Phi_0/(2\pi\mu_0 dJ_c)]^{1/2}$) and the reciprocal Josephson

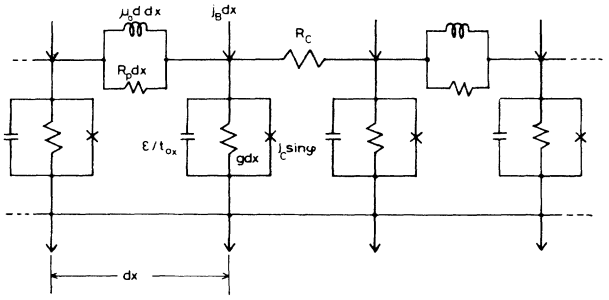

FIG. 1. Equivalent RCJ circuit. Arrow symbols indicate bias-current direction.

plasma frequency ω_J^{-1} ($=[\Phi_0\epsilon/(2\pi J_c t_{ox})]^{1/2}$), respectively. Here $d=\lambda_{L1}+\lambda_{L2}+t_{ox}$ (λ_L is the London penetration depth of the electrodes, t_{ox} is the thickness of the barrier), J_c is the maximum Josephson current density, and ϵ is the dielectric constant of the tunnel barrier. The Josephson plasma period τ_J is defined by $2\pi/\omega_J$. The loss coefficients α and β are represented by $g(\Phi_0 t_{ox}/2\pi J_c\epsilon)^{1/2}$ and $\mu_0\lambda_L\omega_J/R_p$, respectively. Here g is the quasiparticle conductance and R_p is the electrode's parallel resistance due to the quasiparticle excitation. The bias-current coefficient γ is represented by J_B/J_c, where J_B is the bias-current density.

The boundary condition at the coupling resistor can be described by the expressions,

$$\frac{\partial\varphi_1}{\partial x}+\beta\frac{\partial^2\varphi_1}{\partial x\partial t}=\frac{\partial\varphi_2}{\partial x}+\beta\frac{\partial^2\varphi_2}{\partial x\partial t}\ ,$$
$$\frac{\partial\varphi_2}{\partial t}=\frac{\partial\varphi_1}{\partial t}+R_c\left[\frac{\partial\varphi_1}{\partial x}+\beta\frac{\partial^2\varphi_1}{\partial x\partial t}\right]\ , \tag{2}$$

where φ_1 and φ_2 indicate the phase differences for JTL1 and JTL2 at respective sides of the coupling resistor. In these equations, the first one represents the current relationship between the two JTL's, while the second one corresponds to the voltage relationship. Here R_c is normalized by the characteristic impedance Z_0 of the transmission line obtained from Eq. (1) by adopting a small amplitude linear approximation.

The incident fluxons are generated by a voltage pulse input at the JTL1 end. The boundary condition at the input end can be described by the equation

$$\frac{\partial\varphi_1}{\partial t}=V_{ext}(t)+R_{in}\frac{\partial\varphi_1}{\partial x}\ . \tag{3}$$

Here $V_{ext}(t)$ is rectangular input, and its amplitude and duration are normalized by the characteristic voltage V_0 $[=(\Phi_0 J_c t_{ox}/2\pi\epsilon)^{1/2}]$ and the reciprocal plasma frequency, respectively. R_{in} corresponds to the voltage impedance and is also normalized by Z_0. The number of fluxons generated at the input end can be controlled by the amplitude and the duration of the input pulse. The JTL1 and JTL2 length is chosen to be $30\lambda_J$, which is sufficient to form stable fluxons.

B. Threshold properties

Fluxon threshold properties for a single incident fluxon are investigated by integrating the above-modified sine-Gordon equation. The amplitude and duration of the input voltage are chosen to be $3V_0$ and $3/\omega_J$, respectively. Throughout the numerical analysis, the loss coefficients α and β are fixed at 0.004 and 0.028, respectively.

Figure 2 shows the fluxon threshold properties as a function of the respective bias-current levels, γ_1 and γ_2, when R_c is $2.0Z_0$. The solid line indicates the threshold curve of the fluxon transmission, beyond which the incident fluxon transmits across the resistor. Whether the incident fluxon transmits or not depends on both bias-current levels. The dashed line indicates the reflection threshold curve, beyond which the incident fluxon is reflected as an antifluxon. Whether it reflects or not mainly

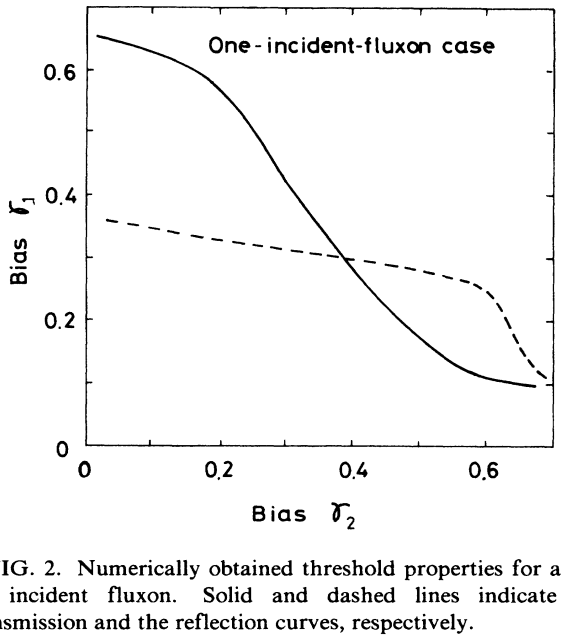

FIG. 2. Numerically obtained threshold properties for a single incident fluxon. Solid and dashed lines indicate the transmission and the reflection curves, respectively.

depends on γ_1. In the high γ_1 and γ_2 region, the incident fluxon can produce both a reflected antifluxon and a transmitted fluxon.

These bias-current dependences can be interpreted in terms of a mechanical analog.[14] In the mechanical analog of a coupled pendulum array, a fluxon corresponds to a 2π rotation of the pendulum array. φ_t and φ_x correspond to angular velocity of the pendulum and torque transmitted by the torsion bar, respectively. According to the above boundary condition, the angular velocity and the torque are transmitted while the angle of the pendulum does not continuously change at the resistor. In most cases, the incident fluxon changes to the damping oscillation in JTL1 as well as in JTL2, because some of the incident energy is reflected, and dissipated at the resistor. The bias current, however, provides the pendulum with external torque density. Therefore, with an increase of γ_2, a new fluxon can be formed in JTL2. With an increase of γ_1, the transmitted and the reflected energy increases, because the incident energy increases. Then a fluxon can be formed in JTL2 even for a small γ_2, and an antifluxon can be generated in JTL1. Consequently, the transmission threshold properties depend on both bias-current levels while the reflection threshold properties mainly depend on γ_1.

Fluxon threshold properties for two incident fluxons are also investigated. The two incident fluxons are generated by the input voltage having a duration of $6/\omega_J$ and an amplitude of $3V_0$. The other parameters of the RCJ are fixed. Figure 3 shows the fluxon threshold properties for the case of two incident fluxons. The threshold curves of the transmission and reflection are shifted to lower bias levels. In this figure, below the solid line and the dashed line, there are two subtransmission and one reflection region surrounded by the solid and dashed lines, respectively. The upper subtransmission region involves the subreflection region. These subtransmission and subreflection

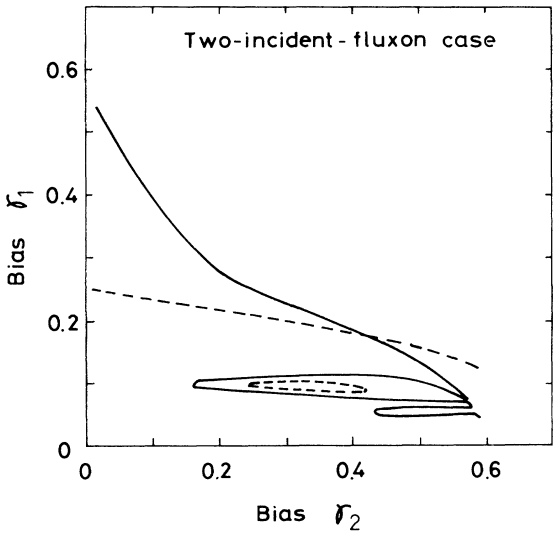

FIG. 3. Numerically obtained threshold properties for two incident fluxons. The areas surrounded by solid and dashed lines correspond to the subtransmission and the subreflection regions, respectively.

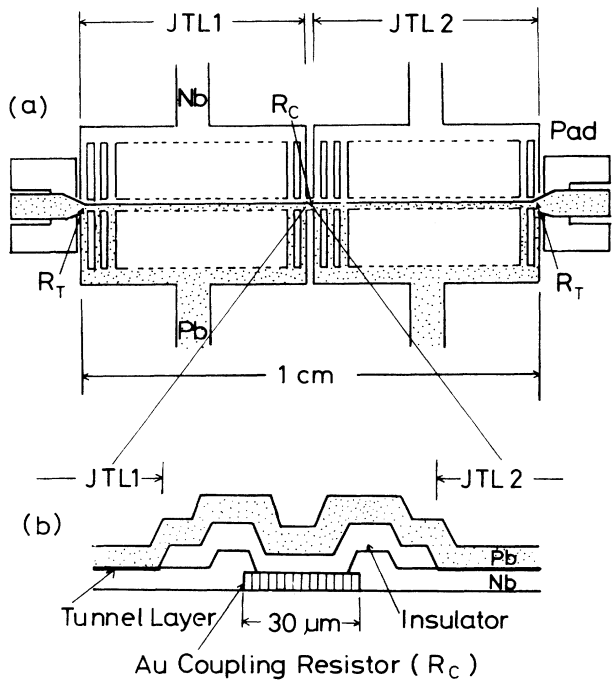

FIG. 4. Fabricated RCJ structure. (a) top view; (b) cross-sectional view at the coupling resistor along the JTL's.

regions mainly depend on γ_1.

As previously discussed, the incident fluxons are more easily transmitted and reflected at the coupling resistor at the higher bias levels. Thus these islandlike subtransmission and subreflection regions contradict the simple interpretation. At the lower bias levels, such as below the solid line, the two incident fluxons change to two damping oscillations that annihilate in JTL2. However, it is found that a new fluxon can be created in the JTL2 under the special condition that the two damping oscillations are in phase.

Since the subtransmission regions correspond to the in-phase condition, as will be discussed in Sec. IV, they are thought to mainly depend on γ_1 which affects the distance between the two incident fluxons. These subtransmission regions are also found when R_c is $0.5,1.0,1.5,2.5Z_0$, while they are never found for the single incident fluxon case. In the previous experiment[13] where R_c was $0.83Z_0$ and α was 0.0036, the subtransmission regions were not observed because such multifluxon effects were not expected and they were not carefully investigated.

III. EXPERIMENT

The RCJ was fabricated on an oxidized silicon wafer by conventional JTL fabrication process.[6,15] The schematic structure is shown in Fig. 4. JTL1 and JTL2 were 25-μm-wide and 5-mm-long Nb/Nb oxide/Pb junctions and were interconnected by a series Au resistor, R_c. The input and output ends were terminated by a Au resistor, R_T. The Au resistors were formed on thin Cr film in order not to be exfoliated by Nb deposition.

The bias currents I_{B1} and I_{B2} are independently provided through comblike electrodes. Each electrode is 50 μm wide and is repeated with a 150-μm period, which is designed to be smaller than a fluxon width. These comblike electrodes act to keep the uniform bias current feeding as a result of the Meissner effect of the superconducting rings formed by adjacent comblike electrodes. The uniformity could be experimentally checked by estimating I_cR_n product of JTL's, where I_c is maximum critical current and R_n is normal resistance component above the gap voltage. However that estimation could not be applied to the present JTL's because R_n's were unknown. To check the uniformity, small monitor junctions were placed in close proximity to the JTL's. There was relatively large difference (about 50%) of the critical current densities between the JTL's and the monitor junctions. It suggests some nonuniformity in Josephson current distribution. All the discrepancy could not be attributed to the effect of nonuniformity because there may be also oxide thickness difference.

The nonuniformity may be caused by a residual external magnetic field.[15] Although there remains some ambiguity in determination of Josephson current density, it does not affect the present results strongly. This is because the provided bias-current level is much larger than the shielding currents caused by residual magnetic field. The external magnetic field is reduced to less than 10^{-3} G by using a μ-metal shield.

I-V characteristics for the two JTL's were measured with their respective bias electrodes, and were almost identical. Josephson current density was determined to be 5.9 Å/cm^2 by using the above I-V characteristics. The Josephson penetration depth and plasma period were estimated at $\lambda_J = 185$ μm and $\tau_J = 138$ ps, respectively. The

quasiparticle tunneling loss coefficient α was estimated at 0.004 by using the linear portion of the monitor junction I-V characteristics around the origin.

R_c and R_T values can be exactly determined by using two different I-V characteristics. The normal resistance value of the I-V characteristics gleaned from the respective Nb electrodes of both JTL's corresponds to $2R_TR_c/(R_c+2R_T)$. On the other hand, the normal resistance component for JTL1 is given by $(R_c + R_T)R_T/(R_c+2R_T)$. By using the above relationships, the coupling resistor and termination resistor were estimated to be $R_c=0.065\ \Omega$ $(=1.29Z_0)$ and $R_T=0.047\ \Omega$ $(=0.92Z_0)$, respectively. In the currently fabricated RCJ, the characteristic impedance is determined to be 0.0503 Ω.

Output voltage responses at the output termination resistor were measured when voltage pulses were fed to the input termination resistor. The measurement system used for observation of single fluxon propagation has previously been described in Ref. 6.

Figure 5 shows observed fluxon waveform examples at the output end as a function of bias-current level, γ_2, where input pulse height $(=-20$ dB) and bias current, γ_1 $(=0.22)$ are fixed. The input pulse height of 560 mV, described in Fig. 5, is set to be 0 dB in the present study. A fluxon was not observed at $(\gamma_1,\gamma_2)=(0.22,0.14)$ and (0.22,0.27), respectively, although it was observed at the lower (0.22,0.07) and the higher (0.22,0.41) bias-current levels. These observed examples show there is an intermediate nontransmission bias region between the high-and low-bias transmission regions.

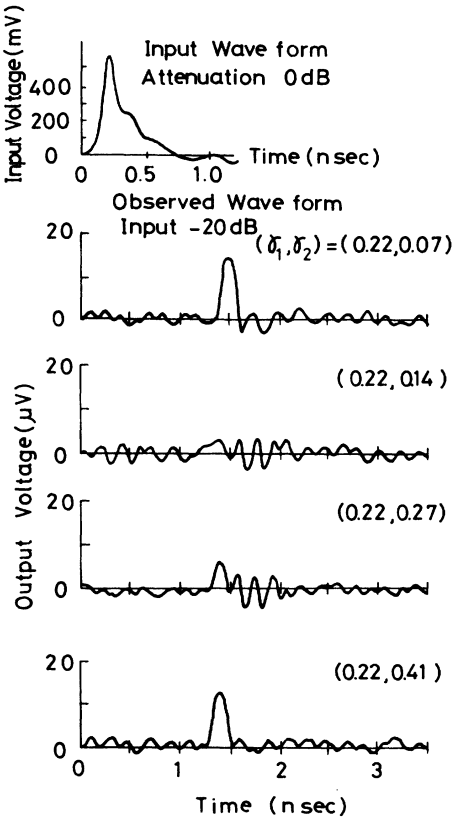

FIG. 5. Observed fluxon waveform examples at the output end as a function of bias γ_2 with fixed input $(=-20$ dB) and γ_1 $(=0.22)$. Input pulse of 0 dB corresponds to 560 mV.

Figure 6 shows the fluxon threshold properties between transmission and nontransmission as a function of the two bias levels (γ_1,γ_2). Open circles, triangles, and squares indicate the transmissions at -20 dB, -23 dB, and -25 dB input, respectively, while solid symbols indicate the nontransmissions. The threshold properties depend on the input pulse height and the respective bias levels. For the higher input pulse case, the incident fluxons transmit across the resistor even at the lower bias levels. At the higher bias levels, the incident fluxons are more easily transmitted through the resistor except for the -20 dB input case.

IV. DISCUSSION

To analyze the experimentally obtained results, Eq. (1) is numerically integrated with a real input waveform and experimentally obtained parameters. The effective input voltage pulse is reduced to a mismatch factor of $2R_T/R_0$, where R_0 is the source impedance. In addition, the voltage is affected by the stray resistance between Nb pad and spring contact, through which the input pulse is fed. Therefore, in numerical simulations of the present RCJ, the termination resistor R_T is treated as a fitting parameter. Here the stray inductance at the coupling resistor must be taken into account. The stray inductance is determined to be 1.5 pH by considering the fabricated structure.

The boundary condition at the coupling resistor can be described by the expression

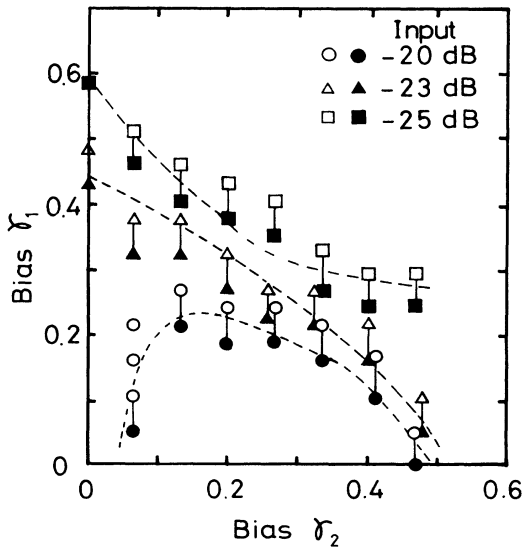

FIG. 6. Experimentally obtained fluxon transmission threshold properties as a function of respective bias currents γ_1 and γ_2. Open circles, triangles, and squares indicate the transmissions at (a) -20 dB, (b) -23 dB, and (c) -25 dB input, respectively. Solid symbols indicate the nontransmissions.

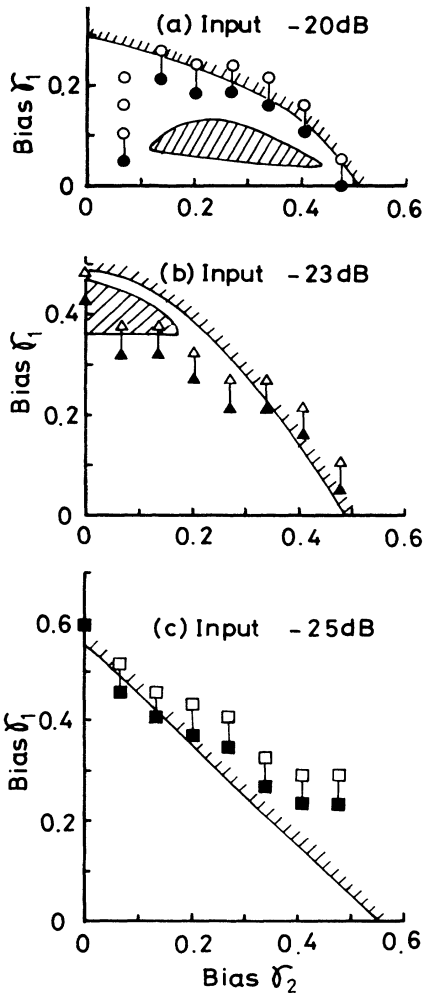

FIG. 7. Comparison between experimental and numerical results on threshold properties. Circles, triangles, and squares correspond to experimental results for −20 dB, −23 dB, and −25 dB input, respectively. Shadowed areas represent the numerically obtained transmission regions.

$$\frac{\partial\varphi_2}{\partial t}=\frac{\partial\varphi_1}{\partial t}+\left[R_c+L_s\frac{\partial}{\partial t}\right]\left[\frac{\partial\varphi_1}{\partial x}+\beta\frac{\partial^2\varphi_1}{\partial x\partial t}\right], \quad (4)$$

where L_s represents the stray inductance component at R_c. The current relationship at the resistor is identical with Eq. (2). The boundary condition at the input end has been described in Ref. 15. Here the rf loss coefficient β cannot be determined experimentally. Therefore, it is assumed to be 0.028, according to Ref. 8. Throughout the following numerical analysis, the termination resistor R_T is chosen to be $0.67Z_0$ as a best fit value. This value means that about 16 Ω stray resistance exists between Nb pad and spring contact.

To compare with the experimentally obtained results, numerically obtained threshold properties are shown in Fig. 7. The shadowed areas represent the numerically obtained transmission regions. Islandlike subtransmission regions surrounded by nontransmission regions are found for the −20 and −23 dB input cases, where more than two fluxons are thought to be generated. Although completely isolated transmission regions were not observed, the numerically obtained threshold properties for −20 and −23 dB input explain the experimental results.

For the −25 dB input case, numerical results did not agree with the experimental ones in a region for γ_1 below 0.28. The experimental results show that in this region the incident fluxon is not transmitted through the coupling resistor even in the high γ_2 region. This suggests that the incident fluxon is either not generated at the input end or it is trapped by a weak pin hole. It is found in the present numerical analysis that the fluxon is not generated at the input end for γ_1 below 0.28 when input is −27 dB.

Figure 8 shows the numerically obtained propagation processes near the coupling resistor as a function of respective bias-current levels with a fixed input of −20 dB. The z axis $(-\partial\varphi/\partial x)$ corresponds to a current distribution (magnetic field) and is normalized by $I_0[=\{\Phi_0 J_c/(2\pi\mu_0 d)\}^{1/2}w]$, where w is the JTL width. In the present experiment I_0 were estimated to be 0.29 mA. $x=0$ corresponds to the position of the coupling resistor. Figures 8(a)–8(f) present fluxon waveform examples as a function of γ_1 with γ_2 fixed and as a function of γ_2 with γ_1 fixed, respectively. These correspond to transmission and nontransmission cases in Fig. 7(a). At lower bias-current levels, two incident fluxons generated at the input end of JTL1 change to damping oscillations in JTL2. However, under the special bias condition that the respective damping oscillations are in phase, a new fluxon can be created in JTL2, as shown in Figs. 8(a) and 8(d). When the respective damping oscillations are out of phase, a fluxon cannot be created in JTL2, as shown in Figs. 8(b) and 8(e). At higher bias-current levels, the second fluxon passes through the coupling resistor, as shown in Figs. 8(c) and 8(f). These propagation processes indicate that an intermediate nontransmission bias region exists between the high- and low-bias transmission regions. The islandlike subtransmission regions in Fig. 7 correspond to these in-phase conditions. The unexpected threshold properties obtained experimentally can be interpreted in terms of this damping oscillation interaction.

In our observation system, the output signals are synchronously added and averaged 1000 times by digital minicomputer systems in order to reduce the noise level. Because of the phase-sensitive nature of the interaction, even small jitters in the input pulse or bias level fluctuation can easily wash out the detailed islandlike structure throughout the averaging process. This explains why completely isolated transmission regions were not observed in our experiment.

These experimentally and numerically obtained threshold properties show that transmission and nontransmission of the incident fluxons at the coupling resistor can be controlled by manipulating the external bias-current levels. This ability to control fluxons is realized by a release from the flux quantization condition at the coupling resistor that enables fluxons to annihilate.

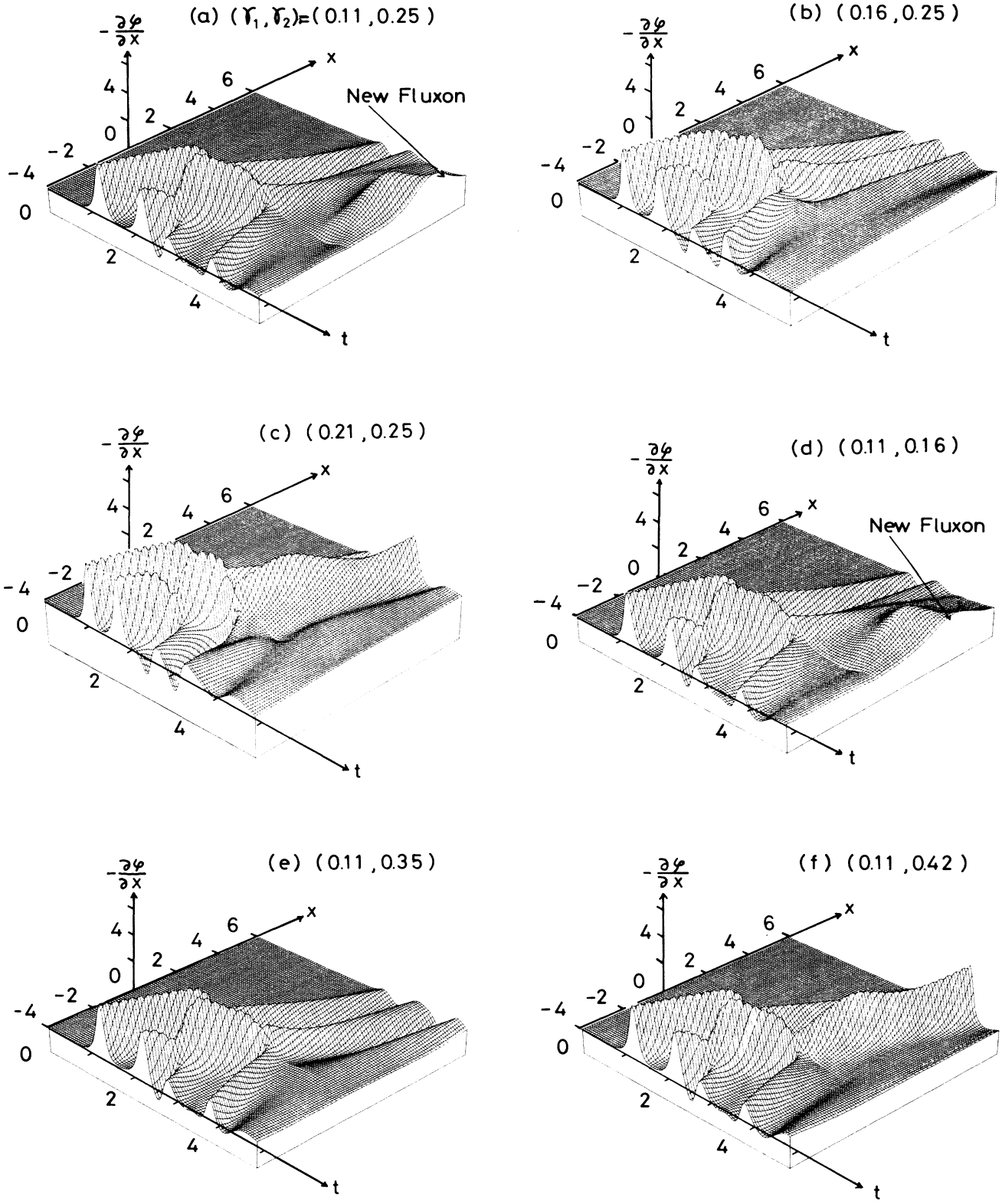

FIG. 8. Numerically obtained propagation processes near the coupling resistor as a function of respective bias-current levels with input fixed at -20 dB. $-\partial\varphi/\partial x$ corresponds to current distribution and is normalized by I_0. Space and time are normalized by Josephson penetration depth and plasma period, respectively. $x=0$ corresponds to the coupling resistor position. (a) (γ_1, γ_2) $=(0.11,0.25)$, (b) (0.16,0.25), (c) (0.21,0.25), (d) (0.11,0.16), (e) (0.11,0.35), and (f) (0.11,0.42).

V. CONCLUSION

Fluxon threshold properties in an RCJ were investigated experimentally and numerically. The fabricated RCJ consisted of two Nb/Nb oxide/Pb JTL's, interconnected by a Au series resistor. Transmitted fluxons at the output end were observed by using a single fluxon observation system. The threshold properties depended on input pulse height and bias levels fed into the respective JTL's. For the higher input case, incident fluxons transmitted across the coupling resistor even at the lower bias levels. While in the higher bias levels, the incident fluxons more easily transmitted through the resistor. However, when two fluxons were generated, an intermediate nontransmission bias region was observed between the high- and low-bias transmission regions. These unexpected threshold properties can be interpreted in terms of the interaction among damping oscillations.

ACKNOWLEDGMENTS

The authors would like to express their thanks to Mr. T. Kawakami and Dr. T. Yamada for their thoughtful comments as well as to Dr. H. Okamoto, Dr. T. Kimura, and Dr. Y. Kato for their continuous support.

[1]A. C. Scott, F. Y. F. Chu, and D. W. McLaughlin, Proc. IEEE **61**, 28 (1973).
[2]A. R. Bishop and T. Schneider, *Soliton and Condensed Matter*, Vol. 8 of *Springer Series of Solid State Sciences* (Springer-Verlag, New York, 1978).
[3]Y. Frenkel and T. Kontorova, J. Phys. (Moscow) **1**, 139 (1939).
[4]V. G. Baryakhtar, B. A. Ivanov, and A. A. Sukstanskii, Zh. Eksp. Teor. Fiz. **79**, 1509 (1980) [Sov. Phys.—JETP **52**, 761 (1980)].
[5]K. Maki, Phys. Rev. B **18**, 1641 (1978).
[6]A. Matsuda and S. Uehara, Appl. Phys. Lett. **41**, 770 (1982).
[7]S. Sakai, H. Akoh, and H. Hayakawa, Jpn. J. Appl. Phys. **21**, L479 (1983).
[8]A. Matsuda and T. Kawakami, Phys. Rev. Lett. **51**, 694 (1983).
[9]J. Nitta, A. Matsuda, and T. Kawakami, J. Appl. Phys. **55**, 2758 (1984).
[10]D. W. McLaughlin and A. C. Scott, Appl. Phys. Lett. **30**, 545 (1977).
[11]D. W. McLaughlin and A. C. Scott, Phys. Rev. A **18**, 1652 (1978).
[12]H. S. Newman and K. L. Davis, J. Appl. Phys. **53**, 7026 (1982).
[13]J. Nitta, A. Matsuda, and T. Kawakami, Appl. Phys. Lett. **44**, 808 (1984).
[14]T. A. Fulton, R. C. Dynes, and P. W. Anderson, Proc. IEEE **61**, 28 (1973).
[15]A. Matsuda, Phys. Rev. B **34**, 3127 (1986).